Chinese Chemical Letters 35 (2024) 109215

Contents lists available at ScienceDirect

Chinese Chemical Letters

journal homepage: www.elsevier.com/locate/cclet

Light/pH dual-responsive magnetic metal-organic frameworks composites for phosphorylated peptide enrichment

Rui Wang[a,1], He Qi[a,1], Haijiao Zheng[a], Qiong Jia[a,b,*]

[a] College of Chemistry, Jilin University, Changchun 130012, China
[b] Key Laboratory for Molecular Enzymology and Engineering of Ministry of Education, School of Life Sciences, Jilin University, Changchun 130012, China

ARTICLE INFO

Article history:
Received 28 June 2023
Revised 19 September 2023
Accepted 15 October 2023
Available online 21 October 2023

Keywords:
Light
pH
Dual-response
Metal-organic frameworks
Phosphorylated peptide

ABSTRACT

Metal-organic frameworks (MOFs) combined with specific ligands are highly adaptable smart materials that can respond to external and physiological stimuli. In this study, we introduced a pyridinyl zwitterionic ligand with light/pH dual response into magnetic MOF composite (Fe_3O_4@ZW-MOF) for enrichment of phosphorylated peptides for the first time. The introduction of the developed ligand gives MOF material dual response properties. Light stimulation affects the generation/disappearance of free radicals of the pyridine derivative, resulting in a change in the charge gradient of the zwitterion, and zwitterion can also regulate the pH of the solution by adding acid or base. Therefore, the reversible capture and release of phosphorylated peptides can be easily achieved by adjusting light and pH. The established phosphorylated peptide enrichment platform exhibits high sensitivity (detection limit of 1 fmol), high selectivity (β-casein:BSA, 1:1000), and good reusability (7 cycles). In addition, the method was applied to the enrichment of phosphorylated peptides in complex systems (non-fat milk and human serum), demonstrating the feasibility of this method for phosphoproteom analysis. In conclusion, the synthesized Fe_3O_4@ZW-MOF is a promising MOF material, which provides the possibility to advance the application of responsive MOFs materials in proteomics.

Metal organic framework (MOFs) are a kind of porous crystal material that assembles metal nodes and organic connectors through strong coordination bonds [1–3]. They have emerged as promising hybrid materials for gas adsorption [4,5], catalysis [6,7], drug delivery [8,9], separation and enrichment [10,11]. Recently, MOFs materials with stimulative responses have been widely concerned. They are highly adaptable and can respond to external as well as physiological stimuli, such as light, temperature, pressure and pH [12,13]. The ability to reversibly "turn on" and "turn off" endows them with a variety of promising applications [14].

Among the various stimuli, pH and light responses of MOFs attract extensive research interests. For instance, Dong *et al.* reported a poly[(2-diethylamino)ethyl methacrylate)] based pH-responsive Pd@MOF-3 material, which is able to trigger the emulsification (at neutral condition) and demulsification (at acidic condition) of toluene droplets by simply adjusting the pH [15]. Light is widely used as a form of physical stimulation because it can provide a fast, clean, remotely controlled state transition [16]. So far, most photoresponsive MOFs materials are skeletons containing azobenzene or dithienylethene [17–19], which can undergo reversible *trans*/*cis*-isomer and open/closed loop structural changes under ultraviolet (UV) or visible light (Vis) irradiation [20]. Pyridine groups can also be used as ligands to build photoresponsive MOFs, such as *N*-substituted pyridines and the more widely known *N*, *N*'-disubstituted 4,4′-bipyridines (viologens) [21,22]. UV/Vis light irradiation can affect their free radical production or disappearance. And their ionic units can act as electron donors and exhibit photo-induced electron transfer behaviors [23].

Compared with single-stimulus responsive materials, dual/multi-stimulus responsive materials tend to be more sensitive to the changes in external environment and more selective to the targets [24,25]. At present, dual-response MOFs materials have been widely used in drug delivery [26,27] and ion detection [28,29]. For instance, Lin *et al.* used acetaldehyde-modified-cystine as a dual-response ligand to synthesize Zr-MOF, forming a functional drug carrier to achieve pH and glutathione (GSH) dual-response drug delivery [26]. Zhang *et al.* developed a semi-rigid V-shaped ligand 3,3′:5′,3″-terpyridine (L) to construct $[Zn_2(L)\ (BDC)_2(H_2O)]_n$, and used as a dual-responsive sensor for detecting TNP and Fe^{3+} in aqueous phase with high efficiency

* Corresponding author.
E-mail address: jiaqiong@jlu.edu.cn (Q. Jia).
[1] These authors contributed equally to this study.

https://doi.org/10.1016/j.cclet.2023.109215
1001-8417/

[28]. Except the above studies, reports about MOFs ligands with dual/multi-stimulus responses are rare, which undoubtedly endow these materials with far-reaching applications in the near future.

Zwitterion is a neutral compound containing both cation and anion in the same molecule [30–32], in which cationic groups include protonated amino, quaternary ammonium, and pyridine units, while anionic groups include carboxylate, sulfonate, and phosphate [33]. Zwitterion has also been employed to construct stimulus-response materials [34]. pH can easily affect the electrostatic interaction between zwitterion and the targets by changing the positive and negative charges carried by zwitterion, and thus zwitterion is generally pH responsive [35]. Pyridinium-based zwitterions have been reported for the construction of photoresponsive MOFs materials [36]. The fact that they can be reversibly photoreduced to a radical species usually leads to the elimination of any charge gradients, and thus can be employed for designing on/off switchable adsorption sites. So far, researches about dual/multi-stimulus response of zwitterion have been seldom reported except Zhou *et al.*' work, in which the intelligent switching effect of zwitterionic poly(carboxybetaine) was explored based on pH and salt concentration dual-response properties [37]. It is of great significance to develop effective dual-responsive zwitterions-based materials for more fascinating applications.

Herein, taking advantages of the stimulus-response properties of zwitterion toward light and pH, we synthesized magnetic MOF adsorbent (Fe_3O_4@ZW-MOF) based on a light/pH dual-responsive zwitterion pyridine derivative ligand. The material was used to establish magnetic solid phase extraction (MSPE) platform for the enrichment of phosphorylated peptides [38–40]. As a common post-translational modification of proteins, protein phosphorylation is involved in many important cellular processes such as cell growth, cycle control and signal transduction pathways [41–44]. Therefore, the detection of phosphorylated peptides is very important [45–47]. Scheme 1 illustrates the preparation process of Fe_3O_4@ZW-MOF and enrichment procedure of phosphorylated peptides. The details of the synthesis of Fe_3O_4@ZW-MOF and the MSPE process of phosphorylated peptides are listed in the supporting information (ESM).

To confirm the successful synthesis of Fe_3O_4@ZW-MOF, FT-IR spectra of H_3LBr_3, Fe_3O_4, and Fe_3O_4@ZW-MOF were determined. In the curve of H_3LBr_3 (Fig. S1 in Supporting information), the peaks at 3402 and 1728 cm^{-1} (characteristic absorption peak of carboxyl groups), 1643 and 1574 cm^{-1} (skeleton vibration of C=C on aromatics), 3040 cm^{-1} (C-H stretching vibration on aromatics), 3117 cm^{-1} (N-H characteristic absorption) exist, proving the successful preparation of H_3LBr_3. In the spectrum of Fe_3O_4 (Fig. 1A), the signal at 586 cm^{-1} can be attributed to the typical absorption peak of Fe-O bond. The spectrum of Fe_3O_4@ZW-MOF shows the peak at 417 cm^{-1} belonging to the characteristic absorption of Zn-O, demonstrating the coordination of metal ions with amphoteric ligands. In addition, the absorption peaks from Fe_3O_4 and H_3LBr_3 are also contained in the spectrum of Fe_3O_4@ZW-MOF, further confirming its successful preparation.

The elemental composition of Fe_3O_4 and Fe_3O_4@ZW-MOF was tested by XPS determination. As shown in Fig. 1B, Fe 2p (712 eV), O 1s (531 eV) and C 1s (285 eV) exist in the curve of Fe_3O_4, fully demonstrating its successful preparation [48]. In addition to the characteristic peaks of Fe_3O_4, the signals of Zn 2p (1022, 1044 eV) and N 1s (400 eV) also appear in the pattern of Fe_3O_4@ZW-MOF, which are raised from Zn and zwitterion pyridine. Additionally, SEM and TEM images of Fe_3O_4 and Fe_3O_4@ZW-MOF (Fig. S2 in Supporting information) show uniform spherical particles with diameters of about 210 and 280 nm, respectively. In summary, the above FT-IR, XPS, SEM and TEM results clearly indicate the successful synthesis of Fe_3O_4@ZW-MOF.

The thermal stability of Fe_3O_4 and Fe_3O_4@ZW-MOF materials was characterized within the temperature range from 30 °C to 800 °C. As shown in Fig. 1C, the TGA curve of Fe_3O_4 displays that the mass of Fe_3O_4 tends to be stable with increasing temperature in the range of 300–550 °C, which is mainly due to the oxidation of Fe_3O_4 to Fe_2O_3. Compared with Fe_3O_4, the TGA analysis of Fe_3O_4@ZW-MOF shows a mass loss of about 36.5%, mainly as a result of the structure collapse of ZW-MOF. The magnetic property of Fe_3O_4@ZW-MOF was investigated by using the magnetic hysteresis loop analysis. As presented in Fig. 1D, the saturation magnetization values of Fe_3O_4 and Fe_3O_4@ZW-MOF are 60.84 and 29.81 emu/g, respectively. The introduction of ZW-MOF reduces the magnetization of the material, but still ensures its rapid recovery from the solution with the aid of an external magnet.

As shown in Fig. 2A, N_2 adsorption-desorption measurements of Fe_3O_4@ZW-MOF indicates the presence of mesoporous structures in the material. According to Brunauer-Emmett-Teller (BET) model, the specific surface area of the material is 121.15 m^2/g. Afterwards, the lattice structure of Fe_3O_4@ZW-MOF was investigated by XRD (Fig. 2B). In addition to the characteristic diffraction peaks of Fe_3O_4 (30.2°, 35.7°, 43.2°, 52.8°, 57.1°, 62.6°) [49], the diffraction peaks of ZW-MOF appear in the lower 2θ range. The

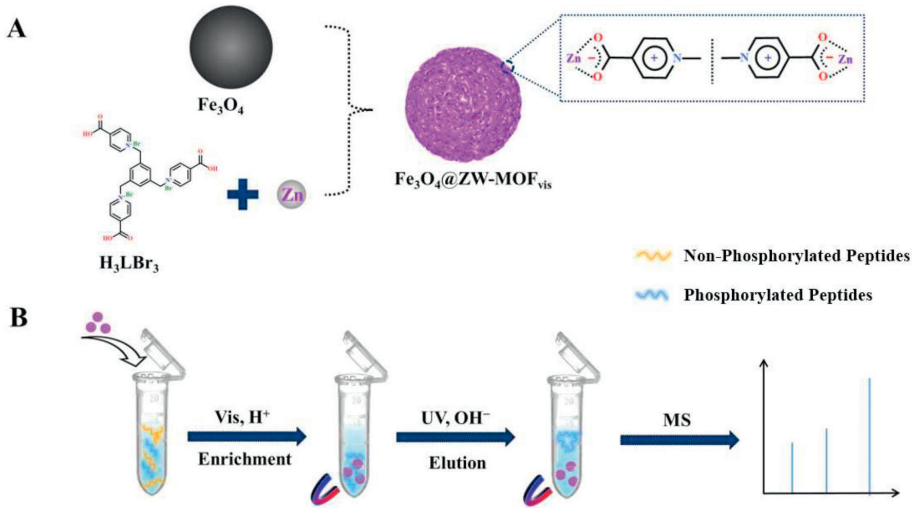

Scheme 1. (A) Synthesis process of Fe_3O_4@ZW-MOF and (B) enrichment process of phosphorylated peptides by Fe_3O_4@ZW-MOF.

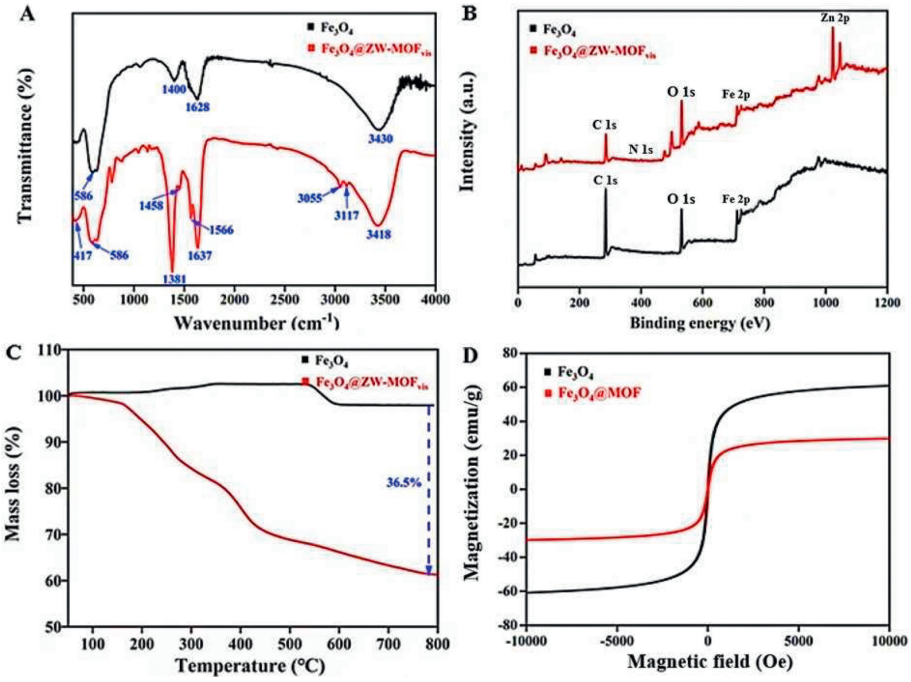

Fig. 1. (A) FT-IR spectra, (B) TGA spectra, (C) XPS patterns, and (D) VSM profiles of Fe_3O_4 and Fe_3O_4@ZW-MOF.

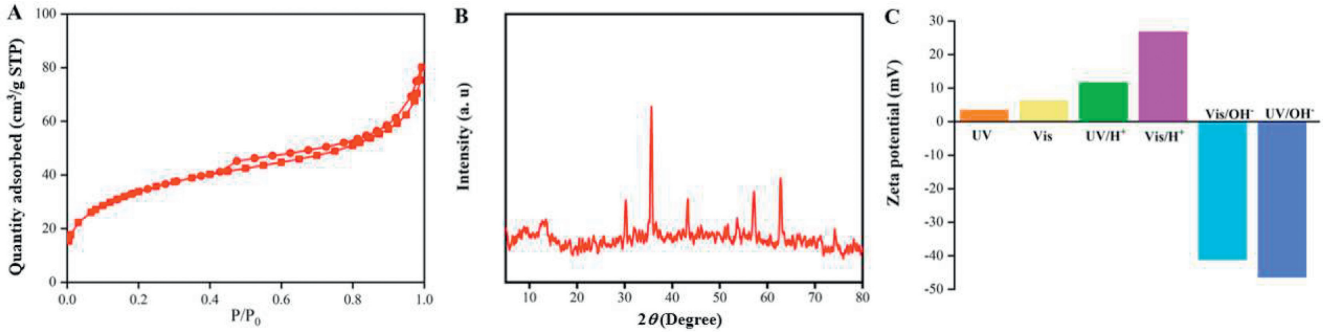

Fig. 2. (A) N_2 adsorption-desorption curve, (B) XRD pattern, and (C) zeta potential values of Fe_3O_4@ZW-MOF.

surface charge states of the materials under different conditions were measured (Fig. 2C). Considering the presence of metal center, the measured zeta potential of the material under UV is +3.4 mV. Under Vis condition, the zeta potential increases to +6.2 mV due to the charged surface generated by MOF. With the introduction of acid, the potential values of the material significantly increase, *i.e.*, +11.6 and +26.7 mV under UV/H^+ and Vis/H^+, respectively. Obviously, the more positive a material is, the higher enrichment capacity toward phosphorylated peptides it possesses. On the contrary, with the introduction of alkali, the potential value of the material drops sharply, and the lowest potential value is −46.3 mV under UV/OH^-. Based on the above results, selective enrichment and elution of phosphorylated peptides can be achieved by simply adjusting light and pH conditions.

The enrichment performance of Fe_3O_4@ZW-MOF toward phosphorylated peptides in β-casein tryptic digest (10 pmol) was investigated (Fig. 3). Figs. 3A and B show the spectra under different irradiation conditions in the same buffer system (acid-free). The number of phosphorylated peptides was higher under Vis irradiation compared with UV condition. When the buffer system was replaced with 70% ACN + 0.1% FA, the intensity at $m/z = 3123$ under Vis irradiation (Fig. 3D) was largely elevated compared with UV irradiation (Fig. S3 in Supporting information). These results indicate that under acid-free condition, Vis irradiation is beneficial for the enrichment of phosphorylated peptides. Under the same UV conditions, when the buffer system is acidic, Fig. 3C shows a higher number of phosphorylated peptides and the intensity of the peak at $m/z = 3123$ is increased by 1.5 times compared with Fig. 3A, indicating that the addition of acid is beneficial for the enrichment of phosphorylated peptides without the influence of light. Under Vis + 70% ACN/0.1% FA, Fig. 3D has the highest intensity (up to 18,000) compared with the other three conditions, and the background of the spectrum is relatively clean. It can also be deduced that Vis and acid are beneficial to the enrichment of phosphorylated peptides by Fe_3O_4@ZW-MOF, which is consistent with the results of the zeta potential values mentioned above.

The sensitivity of the established Fe_3O_4@ZW-MOF based MSPE and mass spectrometry (MS) method was evaluated. Even when the concentration of β-casein digest is as low as 1 fmol, 3 phosphorylated peptides were still detected (Fig. S4 in Supporting information), indicating the high sensitivity of the developed method. The enrichment selectivity of Fe_3O_4@ZW-MOF toward phosphorylated peptides was studied with tryptic digests of β-casein and BSA mixtures with different mass ratios. As shown in Fig. S5 (Supporting information), without the enrichment step, no phosphorylated peptide signals were observed by direct analysis. However, even when the mass ratio of β-casein and BSA is 1:1000, 3 phosphorylated peptide signals were clearly identified, validating

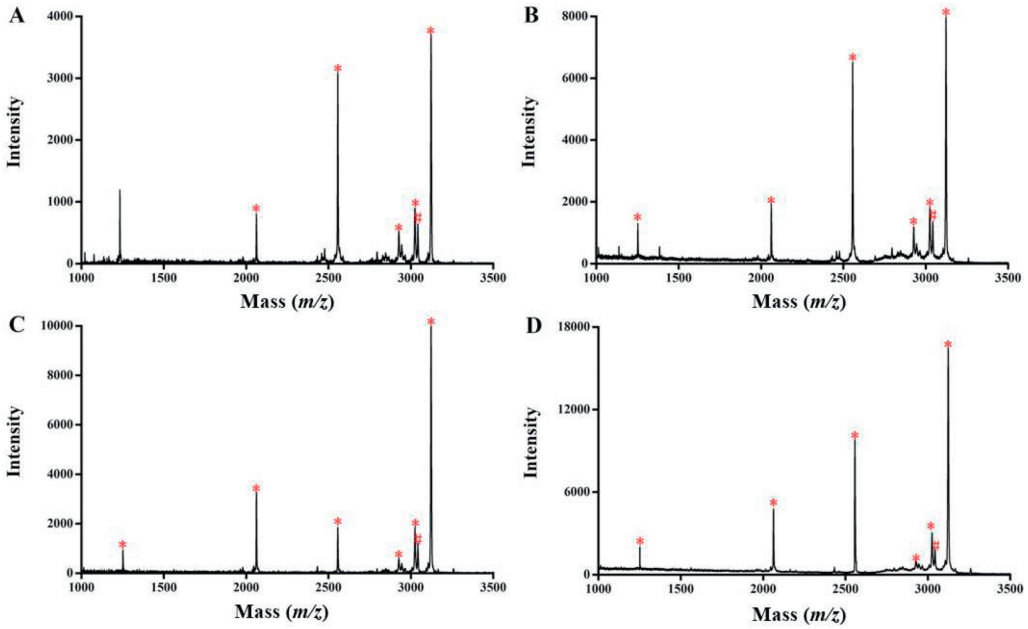

Fig. 3. MALDI-TOF mass spectra of phosphorylated peptides enriched by Fe_3O_4@ZW-MOF under different conditions: (A) UV + 70% ACN; (B) Vis + 70% ACN; (C) UV + 70% ACN/0.1% FA; (D) Vis + 70% ACN/0.1% FA. "*" represents phosphorylated peptide peak, "#" represents dephosphorylated peptide peak, and non-labeled represents non-phosphorylated peptide peak.

the excellent selectivity of Fe_3O_4@ZW-MOF toward phosphorylated peptides.

To study the reusability of Fe_3O_4@ZW-MOF, it was employed to enrich phosphorylated peptides from β-casein tryptic digests for 1, 3, 5, and 7 times. Results displayed in Fig. S6 (Supporting information) demonstrate that there is no significant difference between enrichment properties after the 1st and 7th cycle. It is confirmed that Fe_3O_4@ZW-MOF has good reusability for phosphorylated peptide enrichment. Table S1 (Supporting information) displays the comparison between the prepared Fe_3O_4@ZW-MOF and previously reported materials for phosphorylated peptide enrichment. To deduce, the developed method exhibits the merits of high sensitivity, selectivity and repeatability, and has the potential to be applied to complex biological samples.

Encouraged by the above results, Fe_3O_4@ZW-MOF was used for the enrichment of phosphorylated peptides from complex non-fat milk sample. As for the direct analysis of non-fat milk digests, the signals of phosphorylated peptides were significantly suppressed by the dominant signals of non-phosphorylated peptides (Fig. 4A). However, after enrichment by Fe_3O_4@ZW-MOF, 12 phosphorylated peptides were identified (Fig. 4B). These results indicate that Fe_3O_4@ZW-MOF possesses specificity toward phosphorylated peptides in non-fat milk sample. To further evaluate the applicability of Fe_3O_4@ZW-MOF in practical application, human serum was chosen as another complex biological sample. Direct analysis results without the enrichment step are presented in Fig. 4C, indicating that no phosphorylated peptides signals appear in the MALDI mass spectrum. Nevertheless, after enrichment by Fe_3O_4@ZW-MOF, 4 phosphorylated peptides were identified with high abundance and relatively clean background (Fig. 4D). All the above results confirm that Fe_3O_4@ZW-MOF possesses high enrichment capacity toward phosphorylated peptides and it has great application prospects in complex biological samples.

The mechanism of phosphorylated peptides enrichment by Fe_3O_4@ZW-MOF material was explored. As shown in Fig. S7 (Supporting information), Fe_3O_4@ZW-MOF continues the light response property carried by the zwitterionic ligand, and this light response is mainly due to the formation of photoinduced free radicals. Specifically, an electrostatic field gradient can be generated under Vis condition due to the good intramolecular charge distribution on the surface of the zwitterion ligand. Thus, the obtained Fe_3O_4@ZW-MOF can generate charged organic surfaces in a porous environment. Negatively charged coordination units (carboxyl groups) chelate with metal ions to form MOF material, and positively charged non-coordination units (pyridinyl groups) transfer their charge states to the obtained MOF. Under these conditions, Fe_3O_4@ZW-MOF is positively charged, which is very favorable for the enrichment of negatively charged phosphorylated peptides. In contrast, the zwitterion ligand is capable to reversibly photoreduct free radicals under UV condition. And this phenomenon results in the disappearance of the previously created charge gradient, which eliminates the surface charge of Fe_3O_4@ZW-MOF. At this point, the interaction force between the material and phosphorylated peptides is weakened, thus achieving the release of phosphorylated peptides.

Moreover, the pH response of zwitterion ligand is beneficial to the enrichment of phosphorylated peptides. Under acidic condition (H^+), the protonated pyridine group imparts a positive charge to Fe_3O_4@ZW-MOF, enabling it to specifically capture phosphorylated peptides. Meanwhile, phosphorylated peptides can be released from the surface of Fe_3O_4@ZW-MOF under alkaline condition (OH^-). To sum up, Fe_3O_4@ZW-MOF with light/pH dual-response has excellent enrichment/elution capacity toward phosphorylated peptides. As mentioned above, the results displayed in Figs. 2C and 3 can be interpreted for the enrichment mechanism and confirm the reliability of the mechanism.

In conclusion, this work synthesizes a magnetic MOF with light/pH dual-response based on zwitterionic pyridine ligand. Combined with MS detection, the Fe_3O_4@ZW-MOF based MSPE platform for the separation and enrichment of phosphorylated peptides was established. The MSPE-MS method has a low detection limit, high selectivity and good repeatability, and can identify phosphorylated peptides from complex systems such as non-fat milk and human serum. This study provides some new ideas for the construction of stimulus-responsive MOFs materials, broadens the range of zwitterion applications, and further promotes the development and application of MOFs materials in proteomics.

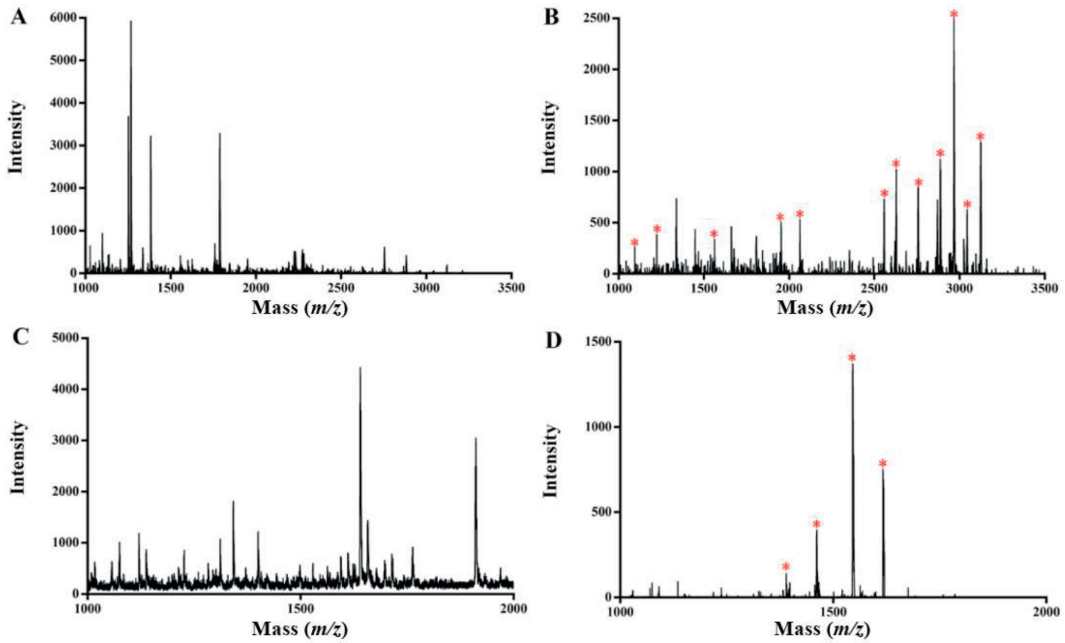

Fig. 4. MALDI-TOF mass spectra of (A, B) tryptic digests of non-fat milk and (C, D) human serum: (A, C) direct detection; (B, D) after Fe_3O_4@ZW-MOF enrichment. "*" represents phosphorylated peptide peak.

Declaration of competing interest

The authors declare that they have no known competing financial interests or personal relationships that could have appeared to influence the work reported in this paper.

Acknowledgments

We acknowledge the financial support of the Fundamental Research Funds for the Central Universities, JLU, China and Open Project of State Key Laboratory of Supramolecular Structure and Materials, Jilin University, China (No. sklssm2022012).

Supplementary materials

Supplementary material associated with this article can be found, in the online version, at doi:10.1016/j.cclet.2023.109215.

References

[1] Stock Norbert, Biswas Shyam, Chem. Rev. 112 (2012) 933–969.
[2] Z. Hu, J. Meng, X. Wang, W. Li, X. Chen, ACS Appl. Mater. Interfaces 12 (2020) 55453–55459.
[3] Z. Xu, H. Chen, H. Chu, et al., Chin. Chem. Lett. 34 (2023) 107829.
[4] Z. Li, X. Shan, P. Yang, et al., Chem. J. Chin. Univ. 40 (2019) 1116–1120.
[5] B. Zheng, F.L. Oliveira, R.N.B. Ferreira, et al., ACS Nano 17 (2023) 5579–5587.
[6] T. Liu, R. Duan, Y. Wang, et al., Chin. Chem. Lett. 33 (2022) 4281–4286.
[7] S. Li, L. Wang, Y. Chen, Chem. J. Chin. Univ. 43 (2022) 20210575.
[8] K. Suresh, A.J. Matzger, Angew. Chem. Int. Ed. 58 (2019) 16790–16794.
[9] Z. Qiao, L. Li, J. Zhou, Chem. J. Chin. Univ. 35 (2014) 2638–2644.
[10] L. Hao, X.L. Liu, J.T. Wang, et al., Chin. Chem. Lett. 27 (2016) 783–788.
[11] M. Yuan, X. Wang, L. Chen, et al., Chem. Res. Chin. Univ. 37 (2021) 679–685.
[12] D. Yan, Z. Wang, Z. Zhang, Acc. Chem. Res. 55 (2022) 1047–1058.
[13] D. Wang, J. Zhou, R. Chen, et al., Chem. Mater. 29 (2017) 3477–3489.
[14] Y. Zhao, Z. Li, J. Ma, ACS Appl. Mater. Interfaces 13 (2021) 55806–55814.
[15] W.L. Jiang, Q.J. Fu, B.J. Yao, et al., ACS Appl. Mater. Interfaces 9 (2017) 36438–36446.
[16] J. Park, L.B. Sun, Y.P. Chen, Z. Perry, H.C. Zhou, Angew. Chem. Int. Ed. 53 (2014) 5842–5846.
[17] L.L. Dang, X.J. Zhang, L. Zhang, et al., J. Coord. Chem. 69 (2016) 1179–1187.
[18] R. Lyndon, K. Konstas, B.P. Ladewig, et al., Angew. Chem. Int. Ed. 52 (2013) 3695–3698.
[19] D. Xu, Y. Zhang, D. Ren, X.B. Chen, Chem. Res. Chin. Univ. 29 (2013) 384–388.
[20] F. Bigdeli, C.T. Lollar, A. Morsali, H.C. Zhou, Angew. Chem. Int. Ed. 59 (2020) 4652–4669.
[21] J. Yu, Y. Cui, H. Xu, et al., Nat. Commun. 4 (2013) 2719–2726.
[22] L.M. Yu, J.J. Fu, S.B. Xia, J.J. Liu, J. Solid State Chem. 305 (2022) 1–6.
[23] Y. Zeng, Z. Fu, H. Chen, et al., Chem. Commun. 48 (2012) 8114–8116.
[24] Y. Zhao, W. Xu, H. Zheng, Q. Jia, Anal. Chem. 95 (2023) 9043–9051.
[25] H. Zheng, Z. Wang, Q. Jia, Small Methods (2023) 2300254.
[26] C. Lin, H. He, Y. Zhang, et al., RSC Adv. 10 (2020) 3084–3091.
[27] J. Dong, K. Ma, Y. Pei, Z. Pei, Chem. Commun. 58 (2022) 12341–12344.
[28] J.F. Zhang, Q.X. Qiu, Q. Xiang, S.M. Ren, C. Zhang, J. Solid State Chem. 294 (2021) 121849.
[29] H. Yang, D. Qi, Z. Chen, et al., J. Solid State Chem. 296 (2021) 121970.
[30] M. Yoshizawa-Fujita, H. Ohno, Chem. Rec. 23 (2023) e202200287.
[31] J. Chen, X. Li, H. Tian, X. Zhu, X. Chen, Chem. J. Chin. Univ. 36 (2015) 2148–2156.
[32] B. Zhao, W. Xu, J. Ma, Q. Jia, Chin. Chem. Lett. 34 (2023) 107498.
[33] K. Qu, Z. Yuan, Y. Wang, et al., ChemPhysMater 1 (2022) 294–309.
[34] Y. Dong, X. Pan, F. Li, D. Yang, Chem. Res. Chin. Univ. 36 (2020) 285–290.
[35] Y. Luo, H. Peng, J. Wu, J. Sun, Y. Wang, Eur. Polym. J. 47 (2011) 40–47.
[36] W. An, D. Aulakh, X. Zhang, et al., Chem. Mater. 28 (2016) 7825–7832.
[37] Z. Miao, Z. Chen, L. Wang, L. Zhang, J. Zhou, J. Mater. Chem. B 10 (2022) 2740–2749.
[38] H. Qi, L. Jiang, Q. Jia, Chin. Chem. Lett. 32 (2021) 2629–2636.
[39] J. Lu, D. Qi, C. Deng, X. Zhang, P. Yang, Nanoscale 2 (2010) 1892–1900.
[40] Y. Chen, H. Chen, C. Yang, et al., Chin. Chem. Lett. 34 (2023) 107352.
[41] V.K.M. Au, Front. Chem. 8 (2020) 708–715.
[42] Y. Hu, Z. Huang, L. Zhou, D. Wang, G. Li, J. Sep. Sci. 37 (2014) 1482–1488.
[43] G. Qing, Q. Lu, Y. Xiong, et al., Adv. Mater. 29 (2017) 1604670.
[44] Z. Xu, Y. Wu, X. Hu, C. Deng, N. Sun, Chin. Chem. Lett. 33 (2022) 4695–4699.
[45] G. Qing, Q. Lu, X. Li, et al., Nat. Commun. 8 (2017) 1482–1488.
[46] X. Li, N. Zhang, R. Tang, et al., Nanoscale 13 (2021) 2923–2930.
[47] H. Chu, H. Zheng, A. Miao, C. Deng, N. Sun, Chin. Chem. Lett. 34 (2023) 107716.
[48] D. Jiang, Z. Li, Q. Jia, Anal. Chim. Acta 1066 (2019) 58–68.
[49] H. Qi, Z. Li, H.J. Zheng, L. Fu, Q. Ji, Chin. Chem. Lett. 30 (2019) 2181–2185.